Proceedings of the 7th World Congress on Civil, Structural, and Environmental Engineering (CSEE'22)
~~Lisbon, Portugal~~ Virtual Conference – April 10 - 12, 2022
Paper No. ICGRE 138
DOI: 10.11159/icgre22.138

Pseudo-Static Analytical Model For The Static And Seismic Stability Of Dry Stone Retaining Walls

Nathanaël Savalle[1], Eric Vincens[2], Paulo B. Lourenço[1]
[1]University of Minho, ISISE, Department of Civil Engineering
Guimarães, Portugal
n.savalle@civil.uminho.pt; pbl@civil.uminho.pt
[2]Université de Lyon, LTDS UMR CNRS 5513, École Centrale de Lyon
36 Avenue Guy de Collongue, 69134 Écully Cedex, France
eric.vincens@ec-lyon.fr

Abstract **-** Dry stone retaining walls are made of rubble stones assembled without mortar. They have shaped many regions worldwide and nowadays constitute a high cultural value, aside from their original operational role (agricultural terraces or transportation networks). However, given their high number and old age, they currently need maintenance, whereas only a few tools are available to assess their stability. In particular, the literature lacks a design tool that accounts for seismic loads. In this paper, a pseudo-static approach based on Coulomb's wedge theory is described in detail. General effects of cohesion, water pore pressure and geometrical features of the backfill are considered. On the other hand, the specificities of dry stone retaining walls are introduced through new parameters, whose values are extracted from laboratory and in-situ experiments.

Keywords**:** Slope stability, Masonry, Earthquake engineering, Coulomb's wedge, Payload, Geotechnical engineering

1. Introduction

Dry stone masonry retaining walls (DSRWs) are made of rubble stones assembled without mortar with definite know-how. They constitute a significant cultural heritage in many regions worldwide. Some emblematic sites have been classified in the UNESCO heritage list (Douro's valley, Portugal or Lavaux's terraces, Switzerland). Most of these structures were built before the twentieth century and therefore require a high level of maintenance today. On the other hand, they bear an important economic role, supporting transporting networks or agricultural terraces. Though abandoned in the middle of the twentieth century for the benefit of steel and concrete materials, dry stone technology recently began to be used again. While fifty years ago, an old DSRW would have been replaced or repaired using concrete, mortar or steel anchors [1]–[3], today, more and more stakeholders choose to rebuild/repair damaged DSRWs engaging specialised dry stone masons. Indeed, their intrinsic low embodied energy, high local social impact, and the small amount of induced waste make them utterly relevant in the global context of sustainable development. In addition, their high cultural value, also enhancing touristic activities (especially in areas literally shaped by dry stone constructions), require their maintenance with original techniques.

Specific research studies regarding dry stone retaining walls (DSRWs) have been mainly conducted in Europe, with experimental [4]–[9], analytical [10]–[17] and numerical works based on the Discrete Element Method (DEM) [18]–[26]. In particular, both free-standing dry stone walls (e.g., [21]), slope retaining walls (e.g., [11]), and road retaining walls (e.g., [19]) have been studied. All the analytical tools already proposed in the literature account for many parameters of actual DSRWs. For example, the various geometrical configurations of the wall-backfill system are considered in almost all analytical studies [10]–[12], [14]–[16]: internal and external batters, as well as the inclination of the retained backfill, are variable. Then, more refinements consider the possibilities to have inclined courses of stones and a different total height between the backfill and the retaining wall [10], [11].

Alejano et al. [12] considered the presence of water pressure through permanent hydrostatic pore pressure. Though pore pressures are hardly expected to accumulate behind a DSRW, it significantly affects the stability of these structures [26]. Preti et al. [27] proposed a more complex hydrological model to account for dynamic pore pressure due to water flows. Though initially excluded from the analytical model developed by Colas et al. [10], [11], the backfill cohesion was added afterwards in the computations presented in the guides for the static design of DSRWs [28]. However, as classically observed for general retaining wall systems, this model does not account for the tension cracks that develop on top of cohesive soils, leading to smaller cohesive forces [29]–[31]. A potential payload placed on the top of the backfill is also accounted for in the analytical model developed by Mundell et al. [16]. Though a vehicle placed on top of a road supported by a retaining wall implies a 3D behaviour not captured by their plane strain model, it allows a conservative estimation of the capacity of DSRWs, when supporting roads. Only Savalle et al. [17] proposed a pseudo-static model for the seismic design of DSRWs, based on the classical Mononobe-Okabe (M-O) method [32], [33]. However, their model does not account for all the previously developed geometrical or mechanical features. Finally, experimental campaigns evidenced the possibility for the stones to internally rotate within a DSRW [4]–[6]. This rotation towards downstream reduces the sliding resistance of DSRWs. This phenomenon happens specifically close to the collapse of the system. Up to now, analytical models do not rigorously take this specificity.

The present paper proposes a unified analytical tool that aims to design dry stone retaining walls for both static and seismic actions through the classical pseudo-static approach (M-O method). It unifies all the improvements present in the analytical models of the literature. Therefore, it accounts for various possible wall-backfill geometries. Similarly, cohesive soils with payloads and water pore pressure acting on the wall are considered, while specificities of DSRWs are also presented. In Section 2, the analytical method is presented, while Section 3 concludes the study with some final remarks.

2. Analytical model for the pseudo-static design of DSRWs

2.1. General framework

The analytical model focuses on slope retaining walls and therefore adopts a plane strain framework. Dry stone retaining walls (DSRWs) are assumed homogeneous so that a single cross-section with the geometrical characteristics presented in Figure 1 models the whole structure. H is the height of the DSRW (above the free surface of the passive soil), while B is its thickness at the base. λ_v represents the external batter of the wall, often taken equal to the inclination of the stone courses α. λ_m corresponds to the internal batter, a relevant parameter for DSRWs built in the Iberian peninsula [12], [26]. Finally, h_f is the height of the supported backfill while β is the slope of the backfill.

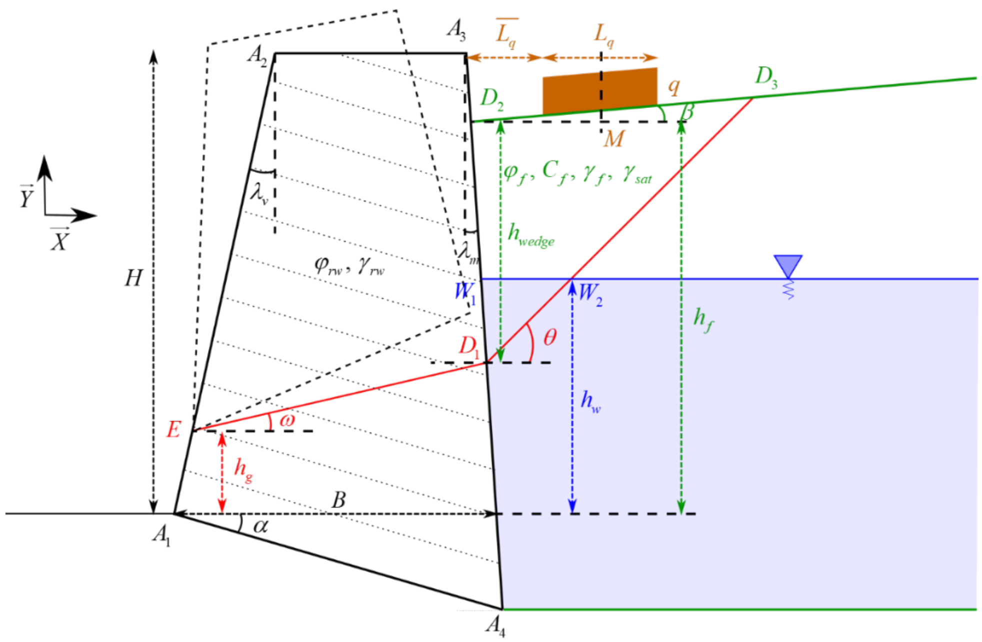

Figure 1: Geometrical and mechanical parameters of a DSRW-backfill system

Both the wall and the backfill are assumed as continua. Its weight γ_f, friction φ_f and cohesion C_f characterise the backfill continuum, while its weight γ_{rw} and friction φ_{rw} characterise the wall continuum. The presence of water on the back of the wall is simply considered through a hydrostatic pore pressure [12], [31], determined by the height of the equivalent column of water h_w: the saturated backfill weight is noted γ_{sat}. The values L_q, $\overline{L_q}$ characterise the payload position (broad modelling of a vehicle for road retaining walls), centred on point M, while q corresponds to its intensity (in kN/m). Finally, the potential failure surface that develops through the wall and the backfill is assumed linear in both media (Figure 2a). Averaging the failure line within the wall is classically done in the literature [6], [10], [12]. Regarding the soil behaviour in the active case, though actual failure lines possess a known log-spiral geometrical shape, the obtained differences with a straight line, assumed here, are minimal [34]. The inclinations ω, θ and position h_g of the failure lines are variable, and their optimisation will be detailed in Section 2.5. The geometrical parameters depicted in Figure 1 are enough to characterise the system entirely; all the other dimensions (e.g., the height of the soil's wedge h_{wedge}) and section areas only depend on these primary features. The last parameter required by the model is the interface friction angle δ that determines the inclination of the earth pressure with respect to the internal wall batter. An interface cohesion C_{int} is also envisioned, though almost always null in practice because of the dry drain placed directly behind a DSRW (see Section 2.2).

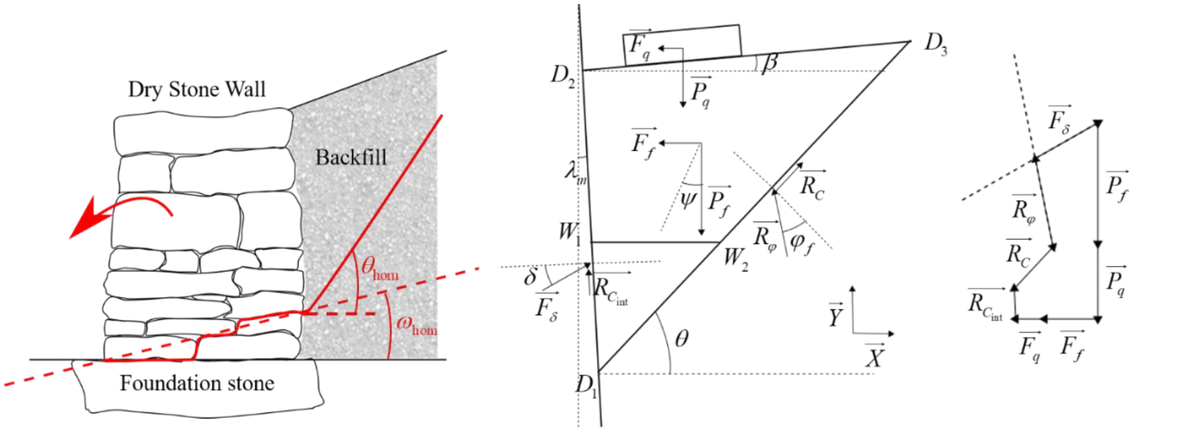

a) Homogenised failure line in the wall/backfill b) Forces applied to the soil's wedge c) Geometrical equilibrium

Figure 2: Homogenised failure lines in the wall and backfill (a) and equilibrium of forces applied to the soil's wedge (b-c)

2.2. Forces applied to the Coulomb soil's wedge

The first part of the analytical model determines the pseudo-static earth pressure $\vec{F_\delta}$ the backfill applies on the wall. Figure 2b describes all the forces acting on the Coulomb's wedge of soil. ψ represents the orientation of the equivalent gravity and is given by the following formula:

$$\tan\psi = \frac{a_h}{1+a_v} \tag{1.1}$$

where a_h and a_v are the horizontal and vertical accelerations expressed in proportion to the natural gravity g. The weight of the soil $\vec{P_f}$, the pseudo-static action of the soil $\vec{F_f}$, the weight of the payload $\vec{P_q}$, the pseudo-static action of the payload $\vec{F_q}$, the cohesive reaction of the soil $\vec{R_C}$, and the cohesive interface force $\vec{R_{C_{\text{int}}}}$ are known and read (Figure 1 & 2):

$$\vec{P_f} = -\gamma_f \times S_{D_1D_2D_3} \times (1+a_v)\vec{Y} \qquad \vec{F_f} = -\gamma_f \times S_{D_1D_2D_3} \times a_h \vec{X} \tag{1.2}$$

$$\vec{P_q} = -q \times L_q \vec{Y} \qquad \vec{F_q} = -q \times L_q \times a_h \vec{X} \tag{1.3}$$

$$\vec{R_C} = \left\|\overrightarrow{D_1D_3}\right\| \times C_f \times \left(\cos\theta\vec{X} + \sin\theta\vec{Y}\right) \tag{1.4}$$

$$\vec{R_{C_{\text{int}}}} = \left\|\overrightarrow{D_1D_2}\right\| \times C_{\text{int}} \times \left(\sin\lambda_m\vec{X} + \cos\lambda_m\vec{Y}\right) \tag{1.5}$$

In the equations above, the soil's wedge area $S_{D_1D_2D_3}$ and lengths $\left\|\overrightarrow{D_1D_3}\right\|$ and $\left\|\overrightarrow{D_1D_2}\right\|$ only depend on the basic geometrical parameters described in Figure 1. The intensities of the frictional reaction of the stable backfill $\vec{R_\varphi}$ and the wall reaction (the opposite of earth pressure) $\vec{F_\delta}$ are unknown though their directions are given, assuming limit equilibrium conditions:

$$\vec{F_\delta} = \left\|\vec{F_\delta}\right\| \times \left(\cos(\delta+\lambda_m)\vec{X} + \sin(\delta+\lambda_m)\vec{Y}\right) \quad \vec{R_\varphi} = \left\|\vec{R_\varphi}\right\| \times \left(-\sin(\theta-\varphi_f)\vec{X} + \cos(\theta-\varphi_f)\vec{Y}\right) \tag{1.6}$$

In case water pore pressures exist (i.e., line (W_1W_2) inside the wedge $(D_1D_2D_3)$), Eq. (1.2) becomes:

$$\vec{P_f} = \left[-\gamma_f \times \left(S_{D_1D_2D_3} - S_{D_1W_1W_2}\right) - (\gamma_{sat} - \gamma_w) \times S_{D_1W_1W_2}\right] \times (1+a_v)\vec{Y} \tag{1.7}$$

$$\vec{F_f} = \left[-\gamma_f \times \left(S_{D_1D_2D_3} - S_{D_1W_1W_2}\right) - (\gamma_{sat} - \gamma_w) \times S_{D_1W_1W_2}\right] \times a_h \vec{X} \tag{1.8}$$

Classically, when cohesive soils are accounted for, retained backfills experience vertical cracks starting from the free surface. Indeed, following the classical Rankine's theory and using the classical active earth pressure coefficient K_a [35], the normal stress at a depth h applied by the backfill to the wall is given by:

$$\sigma_H(h) = K_a \times \sigma_v(h) - 2C_f \times \sqrt{K_a} = K_a \times \gamma_f h - 2C_f \times \sqrt{K_a} \tag{1.9}$$

For small depths h, $\sigma_h(h)$ becomes negative, which means that the backfill retains the wall. However, it does not happen in practice and leads to vertical cracks in the soil up to the depth of the tension cracks, called h_c, which, according to Rankine's theory, is equal to:

$$h_c = \frac{2C_f}{\gamma_r \times \sqrt{K_a}} \tag{1.10}$$

Eq. (1.10) accounts neither for an inclined earth pressure (along an angle δ) nor for pseudo-static actions. Therefore, in this work, the formula given by Lin et al. is preferred [30]:

$$h_c = \frac{a_2 \times C_{\text{int}} \times \cos\psi - a_3 \times C_f \times \cos\psi}{a_1 \times \gamma_f \times (1+a_v)} - \frac{q}{\gamma_f} \tag{1.11}$$

$$a_1 = \frac{\cos\left(\varphi_f + \pi/2 - \theta - \psi\right) \times \left[\cos\left(\beta + \pi/2 - \theta\right) \times \sin\left(\lambda_m + \psi\right) + \cos\left(\lambda_m - \beta\right) \times \sin\left(\psi - \pi/2 + \theta\right)\right]}{\cos\left(\pi/2 - \theta + \beta\right) \times \left[\sin\left(\beta + \varphi_f + \pi/2 - \theta - \lambda_m - \delta - \psi\right) + \cos\left(\varphi_f + \pi/2 - \theta + \lambda_m + \delta\right) \times \sin\left(\beta + \psi\right)\right]},$$

$$a_2 = \frac{\cos\left(\beta + \varphi_f + \pi/2 - \theta - \lambda_m - \psi\right) + \sin\left(\lambda_m + \varphi_f + \pi/2 - \theta\right) \times \sin\left(\beta + \psi\right)}{\sin\left(\beta + \varphi_f + \pi/2 - \theta - \lambda_m - \delta - \psi\right) + \cos\left(\varphi_f + \pi/2 - \theta + \lambda_m + \delta\right) \times \sin\left(\beta + \psi\right)},$$

$$a_3 = \frac{\cos\left(\lambda_m - \beta\right) \times \cos\left(\beta + \psi\right) \times \cos\varphi_f}{\cos\left(\pi/2 - \theta + \beta\right) \times \left[\sin\left(\beta + \varphi_f + \pi/2 - \theta - \lambda_m - \delta - \psi\right) + \cos\left(\varphi_f + \pi/2 - \theta + \lambda_m + \delta\right) \times \sin\left(\beta + \psi\right)\right]} \tag{1.12}$$

a_1, a_2 and a_3 represent constants that depend on all the geometrical angles of the problem [30]. Once h_c is identified, the cohesion value along $\left(D_1D_3\right)$ is reduced according to Figure 3, and Eq. (1.4) becomes:

$$\overrightarrow{R_C} = \left[\left\|\overrightarrow{D_1D_c}\right\| \times C_f + \left\|\overrightarrow{D_cD_3}\right\| \times C_f/2\right] \times \left(\cos\theta\overrightarrow{X} + \sin\theta\overrightarrow{Y}\right) \tag{1.13}$$

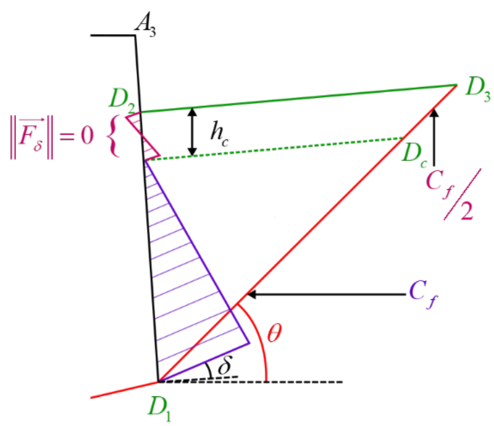

Figure 3: Depth of the tension cracks and how the analytical model accounts for it

In fact, it consists of ensuring that up to the depth h_c, the wall supports no earth pressure from the backfill, with the assumption of a linear distribution of earth pressure, as commonly done in geotechnics [35]. Theoretically, a similar reduction should also be applied to the cohesive interface reaction (Eq. (1.5)). However, as already mentioned, this component is always null for DSRWs because of their gravel drain; a refinement of Eq. (1.5) is thus not relevant.

2.3. Equilibrium of the Coulomb's wedge: determination of the earth pressure $\overrightarrow{F_\delta}$

Gathering all the forces applied to the soil's wedge expressed in Eqs. (1.3), (1.5), (1.6), (1.7), (1.8) and (1.13), and writing the force equilibrium along the direction $\cos(\theta-\varphi_f)\overrightarrow{X}+\sin(\theta-\varphi_f)\overrightarrow{Y}$ to nullify the contribution of $\overrightarrow{R_\varphi}$ in Eq. (1.6), one can obtain the intensity of the earth pressure:

$$\left\|\overrightarrow{F_\delta}\right\|=\frac{\left(\left\|\overrightarrow{P_f}\right\|+\left\|\overrightarrow{P_q}\right\|\right)\sin(\theta-\varphi_f)+\left(\left\|\overrightarrow{F_f}\right\|+\left\|\overrightarrow{F_q}\right\|\right)\cos(\theta-\varphi_f)-\left\|\overrightarrow{R_C}\right\|\cos\varphi_r-\left\|\overrightarrow{R_{C_{\text{int}}}}\right\|\sin(\theta-\varphi_r-\lambda_m)}{\cos(\lambda_m+\delta+\varphi_f-\theta)} \tag{1.14}$$

The last unknown that needs to be determined is the application point of the earth pressure y_δ. In the classical case without cohesion, pore pressure, payload or seismic actions, the application point can be calculated at a depth $y_\delta=1/3\times h_{wedge}$ (Figure 4a). Whenever pore pressures are considered within the soil's wedge, application point depth decreases following the weighted equation:

$$y_\delta=\frac{1/3\times h_{wedge}\times\gamma_f\times S_{D_1D_2D_3}+1/3\times\left(h_w-\left(h_f-h_{wedge}\right)\right)\times\left(\gamma_{sat}-\gamma_w-\gamma_f\right)\times S_{D_1W_1W_2}}{\gamma_f\times S_{D_1D_2D_3}+\left(\gamma_{sat}-\gamma_w-\gamma_f\right)\times S_{D_1W_1W_2}} \tag{1.15}$$

Classically, when accounting for cohesive soils, the height of the application point of earth pressure diminishes. One can find in a simple case without payload and seismic actions that the application point is located at a height y_δ, given by the following equation:

$$y_\delta=\frac{\gamma_f\sin(\theta-\varphi_f)\cos(\theta)h_{wedge}^2-3C_f\cos\varphi_f h_{wedge}}{3\gamma_f\sin(\theta-\varphi_f)\cos(\theta)h_{wedge}-6C_f\cos\varphi_f} \tag{1.16}$$

In fact, though the application point should not theoretically move when adding pseudo-static actions, the experimental literature found some variations depending on the displacement mode of the wall. In particular, the application point of the dynamic increment can be located higher in the walls, up to $0.7h_f$ [36], [37]. Considering a wall displacement mode with a mixed translation and rotation about its base, very close to the behaviour of DSRWs, Ishibashi and Fang found that the dynamic increment of earth pressure is located at $0.5h_f$ [36]. As recommended in the Eurocode, this last value is considered here (either for the soil's wedges $(D_1D_2D_3)$ and $(D_1W_1W_2)$ see example Figure 4b). The earth pressure static and dynamic increments due to the payload are assumed to act at point N, projection point of M (middle of the payload) parallel to the failure line (Figure 4c).

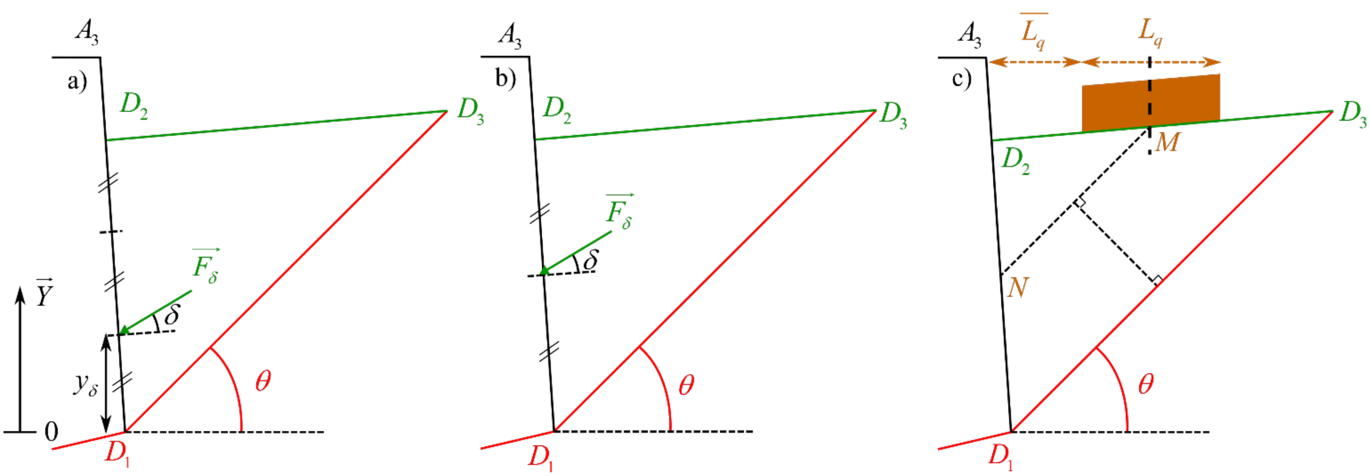

Figure 4: Application point of the earth pressure in some particular cases: a) only static action of the soil; b) only seismic action of the soil, and c) only static action of the payload

The application points of the earth pressure are known if every single destabilising force ($\overrightarrow{P_f}$ considering the effect of water and cohesion ($\overrightarrow{R_C}$), $\overrightarrow{P_q}$, $\overrightarrow{F_f}$, or $\overrightarrow{F_q}$) is considered separately. The final application point is computed through a weighting formula, with the destabilising force intensities ($\left\|\overrightarrow{P_f}\right\|$, $\left\|\overrightarrow{P_q}\right\|$, $\left\|\overrightarrow{F_f}\right\|$, $\left\|\overrightarrow{F_q}\right\|$) as weights. Note that the exact position of the application point of the cohesive reaction $\overrightarrow{R_{C_{\text{int}}}}$ is not needed since its line of thrust is known and is already enough to compute the wall's equilibrium. As a final remark, the stabilising effect of $\overrightarrow{R_{C_{\text{int}}}}$ on the application point of earth pressure $\overrightarrow{F_\delta}$ is not considered, $\overrightarrow{R_{C_{\text{int}}}}$ being null in most cases and the assumption being conservative.

2.4. Equilibrium of the DSRW

Figure 5 focuses on the stability of a given wall section $(EA_2A_3D_1)$. The failure line (ED_1) crosses the DSRW through the dry joints. $\overrightarrow{P_{rw}}$ is the weight of the wall, $\overrightarrow{F_{rw}}$ is the wall pseudo-static action, $\overrightarrow{F_w}$ is the water force. $\overrightarrow{F_\delta}$ is the earth pressure and $\overrightarrow{R_{C_{\text{int}}}}$ is the cohesive interface force, both evaluated in Section 2.3 and finally $\overrightarrow{R_b}$ corresponds to the action transmitted to the foundation. They read:

$$\overrightarrow{P_{rw}} = -\gamma_{rw} \times S_{EA_2A_3D_1} \times (1+a_v)\overrightarrow{Y},\ \overrightarrow{F_{rw}} = -\gamma_{rw} \times S_{EA_2A_3D_1} \times a_h \overrightarrow{X},\ \overrightarrow{F_w} = -\gamma_w \times \frac{(h_w - h_f + h_{wedge})^2}{2}\overrightarrow{X} \qquad (1.17)$$

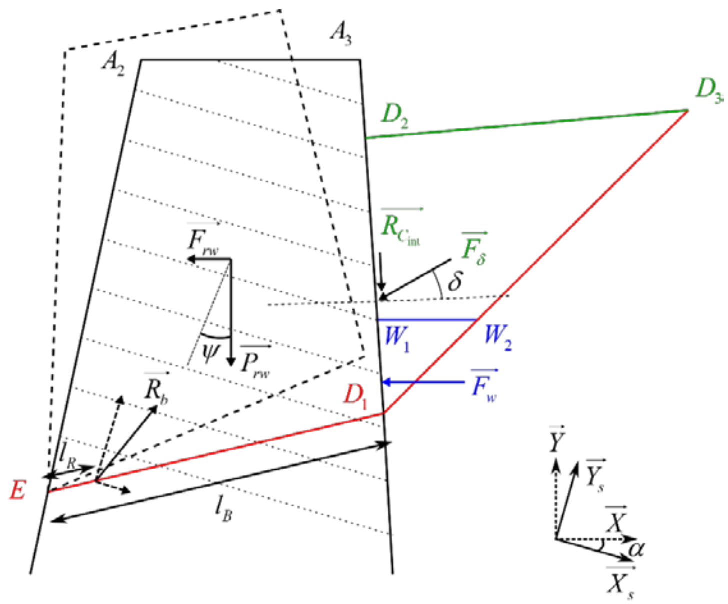

Figure 5: Equilibrium of the wall section $S_{EA_2A_3D_1}$

Forces $\overrightarrow{P_{rw}}$ and $\overrightarrow{F_{rw}}$ are applied at the centre of gravity of the studied wall section $S_{EA_2A_3D_1}$, while $\overrightarrow{F_w}$ is applied at one-third of the height of the triangle $(D_1W_1W_2)$. The stability of the section is then computed in both sliding and overturning failure mechanisms. Overturning is prevented if the moment of the destabilising forces ($\overrightarrow{F_{rw}}$, $\overrightarrow{F_w}$ and $\overrightarrow{F_\delta}$) is smaller than that of stabilising forces ($\overrightarrow{P_{rw}}$ and eventually $\overrightarrow{R_{C_{\text{int}}}}$). It corresponds to checking that the application point of the reaction force $\overrightarrow{R_b}$ lies within the line (ED_1). The sliding equilibrium is based on the dry contact friction resistance between courses of stones. First, the equilibrium along $\overrightarrow{X}$ and $\overrightarrow{Y}$ directions gives the intensity of the base reaction $\overrightarrow{R_b}$, which is then projected in directions $\overrightarrow{X_s}$ and $\overrightarrow{Y_s}$, parallel and respectively perpendicular to the stone bed's inclination α. Then, the classical Mohr-Coulomb criterium is computed:

$$\overrightarrow{R_b} \cdot \overrightarrow{X_s} < \overrightarrow{R_b} \cdot \overrightarrow{Y_s} \times \tan\varphi_{rw} \qquad (1.18)$$

As mentioned earlier, DSRWs are also characterised by the possibility for stones to rotate when loaded, given DSRW's porosity [4]–[6]. From real DSRWs tested during the experimental campaigns of Colas et al. [4], [5] and Villemus et al. [6], all the walls that fell purely in sliding had an eccentricity of the base reaction $\overrightarrow{R_b}$, equal to $e_b = 1 - l_R/l_B \approx 0.3$ (Figure 5). These walls also displayed local rotations of stones. Though specific full-scale tests should confirm it, $e_b \approx 0.3$ seems to play a critical role in the local rotation of stones. The more the stones are loaded far from the central part of the wall/stones, the more they tend to rotate and rearrange their system of contact points. The internal rotation of stones is called η and, according to these experiments, can be taken between 5º and 10º. Eq. (1.18) becomes:

$$\overrightarrow{R_b} \cdot \overrightarrow{X_s} < \overrightarrow{R_b} \cdot \overrightarrow{Y_s} \times \tan\left(\varphi_{rw} - \eta\right) \tag{1.19}$$

To account for the influence of the eccentricity, the authors propose to fully activate the internal rotation $\eta_{mob} = \eta$ when the eccentricity is greater than $e_b > 0.3$. On the contrary, no rotation ($\eta_{mob} = 0^{\mathrm{o}}$) is activated when the eccentricity is less than $e_b < 0.25$. Between these two thresholds, a linear weighting function is used:

$$\eta_{mob} = \eta \frac{e_b - 0.25}{0.3 - 0.25} \tag{1.20}$$

2.5. Optimisation of the stability: find the actual failure line

After both sliding and overturning stabilities are expressed depending on the system's parameters and the unknows of the failure line (h_g, ω and θ), one can optimise these three parameters to find the most critical situation, determining the factors of safety. One should note that the optimisation should be done for both sliding and overturning phenomena, leading to two sets of optimised failure line parameters ($h_{g,opt}$, ω_{opt} and θ_{opt}).

As noted by several authors, the inclination ω is crucial for the overturning stability and is also constrained by the arrangement of stones ($\omega_{opt} < \omega_{\max}$, see Figure 2a) [12], [17], [26]. The formula $\tan\omega_{\max} = h_u / b_u$ has been proposed recently [17], with h_u and b_u the mean height and length, respectively, of stone units. It leads to $\omega_{\max} \approx 20^{\mathrm{o}}$ for DSRWs assembled with rubble stones [4]–[6], [17], and a bit larger values $\omega_{\max} \approx 25 - 45^{\mathrm{o}}$ for DSRWs built with higher units [26].

4. Conclusion

In summary, the present work proposes a unified methodology to design slope dry stone masonry retaining walls. It accounts for almost all idealised geometries. The effect of eventual payloads, water pore pressure, as well as soil cohesion and the associated tension cracks, are included. Similarly, seismic actions are modelled through the classical pseudo-static approach. However, it is reminded that permanent payloads and water accumulation behind DSRWs need to be prevented. Another improvement of the paper is that it proposes an analytical formula and a practical methodology to introduce the internal rotation of stones when the DSRW is loaded. The latter states that the rotation occurs when the loads are concentred in the downstream part of the DSRW, forcing stones to rearrange themselves locally to find new contacts. Dedicated full-scale experiments are envisioned to assess the validity of this proposal. Finally, the above-presented tool allows doing complete parametric analysis to support the design of such structures, being very fast to run.

Acknowledgements

The authors want to acknowledge the French Ministry of Education and Research for their financial support through a PhD grant attributed to the first author. This work was also partly financed by FCT / MCTES through national funds (PIDDAC) under the R&D Unit Institute for Sustainability and Innovation in Structural Engineering (ISISE), under reference UIDB / 04029/2020. Finally, it has been partly funded by the STAND4HERITAGE project (new standards for seismic assessment of built cultural heritage) that has received funding from the European Research Council (ERC) under the European Union's Horizon 2020 research and innovation programme (Grant agreement No. 833123), as an Advanced Grant. Its support is gratefully acknowledged. The opinions and conclusions presented in this paper are those of the authors and do not necessarily reflect the views of the sponsoring organisations.

References

[1] D. A. Bruce and R. A. Jewell, 'Soil nailing: application and practice-part 1', *Ground Eng.*, vol. 19, no. 8, pp. 10–15, 1986.
[2] C. J. F. P. Jones, 'Current practice in designing earth retaining structures', *Ground Eng.*, vol. 12, no. 6, 1979.
[3] C. J. F. P. Jones, *Dry stone walls in the maintenance of brick and stone masonry structures*. E&FN Spon, 1990.
[4] A.-S. Colas, J.-C. Morel, and D. Garnier, 'Assessing the two-dimensional behaviour of drystone retaining walls by full-scale experiments and yield design simulation', *Géotechnique*, vol. 63, no. 2, pp. 107–117, 2013.
[5] A.-S. Colas, J.-C. Morel, and D. Garnier, 'Full-scale field trials to assess dry-stone retaining wall stability', *Eng. Struct.*, vol. 32, no. 5, pp. 1215–1222, 2010.

[6] B. Villemus, J.-C. Morel, and C. Boutin, ‘Experimental assessment of dry stone retaining wall stability on a rigid foundation’, *Eng. Struct.*, vol. 29, no. 9, pp. 2124–2132, 2006.
[7] H. H. Le, J.-C. Morel, A.-S. Colas, B. Terrade, and D. Garnier, ‘Assessing the Three-Dimensional Behaviour of Dry Stone Retaining Walls by Full-Scale Experiments’, *Int. J. Archit. Herit.*, vol. 14, no. 9, pp. 1373–1383, 2020.
[8] C. Mundell, P. McCombie, A. Heath, and J. Harkness, ‘Behaviour of drystone retaining structures’, *Proc. Inst. Civ. Eng. Struct. Build.*, vol. 163, no. 1, pp. 3–12, 2010.
[9] N. Savalle, J. Blanc-Gonnet, E. Vincens, and S. Hans, ‘Dynamic behaviour of drystone retaining walls: shaking table scaled-down tests’, *Eur. J. Environ. Civ. Eng.*, pp. 1–21, 2020.
[10] A.-S. Colas, J.-C. Morel, and D. Garnier, ‘Yield design of dry-stone masonry retaining structures - Comparisons with analytical, numerical, and experimental data’, *Int. J. Numer. Anal. Methods Geomech.*, vol. 32, no. 14, pp. 1817–1832, 2008.
[11] A.-S. Colas, J.-C. Morel, and D. Garnier, ‘Yield design modelling of dry joint retaining structures’, *Constr. Build. Mater.*, vol. 41, pp. 912–917, 2013.
[12] L. R. Alejano, M. Veiga, J. Taboada, and M. Díez-Farto, ‘Stability of granite drystone masonry retaining walls: I. Analytical design’, *Géotechnique*, vol. 62, no. 11, pp. 1013–1025, 2012.
[13] Z. Li, Y. Zhou, and Y. Guo, ‘Upper-Bound Analysis for Stone Retaining Wall Slope Based on Mixed Numerical Discretization’, *Int. J. Geomech.*, vol. 18, no. 10, pp. 1–14, 2018.
[14] B. Terrade, A.-S. Colas, and D. Garnier, ‘Upper bound limit analysis of masonry retaining walls using PIV velocity fields’, *Meccanica*, vol. 53, no. 7, pp. 1661–1672, 2018.
[15] H. H. Le, D. Garnier, A.-S. Colas, B. Terrade, and J.-C. Morel, ‘3D homogenised strength criterion for masonry: Application to drystone retaining walls’, *J. Mech. Phys. Solids*, vol. 95, pp. 239–253, 2016.
[16] C. Mundell, P. McCombie, C. Bailey, A. Heath, and P. Walker, ‘Limit-equilibrium assessment of drystone retaining structures’, *Proc. Inst. Civ. Eng. Geotech. Eng.*, vol. 162, no. 4, pp. 203–212, 2009.
[17] N. Savalle, E. Vincens, and S. Hans, ‘Pseudo-static scaled-down experiments on dry stone retaining walls: Preliminary implications for the seismic design’, *Eng. Struct.*, vol. 171, pp. 336–347, Sep. 2018.
[18] J. J. Oetomo, E. Vincens, F. Dedecker, and J.-C. Morel, ‘Modeling the 2D behavior of dry-stone retaining walls by a fully discrete element method’, *Int. J. Numer. Anal. Methods Geomech.*, vol. 40, no. 7, pp. 1099–1120, 2016.
[19] J.-C. Quezada, E. Vincens, R. Mouterde, and J.-C. Morel, ‘3D failure of a scale-down dry stone retaining wall : a DEM modelling’, *Eng. Struct.*, vol. 117, pp. 506–517, 2016.
[20] N. Savalle, É. Vincens, and S. Hans, ‘Experimental and numerical studies on scaled-down dry-joint retaining walls: Pseudo-static approach to quantify the resistance of a dry-joint brick retaining wall’, *Bull. Earthq. Eng.*, vol. 18, pp. 581–606, Jan. 2020.
[21] P. J. Walker and J. G. Dickens, ‘Stability of medieval dry stone walls in Zimbabwe’, *Géotechnique*, vol. 45, no. 1, pp. 141–147, 1995.
[22] P. Walker, P. McCombie, and M. Claxton, ‘Plane strain numerical model for drystone retaining walls’, *Proc. Inst. Civ. Eng. - Geotech. Eng.*, vol. 160, no. 2, pp. 97–103, 2007.
[23] M. Claxton, R. A. Hart, P. F. McCombie, and P. J. Walker, ‘Rigid block distinct-element modelling of dry-stone retaining walls in plane strain’, *ASCE J. Geotech. Geoenvironmental Eng.*, vol. 131, no. 3, pp. 381–389, 2005.
[24] W. Powrie, R. M. Harkness, X. Zhang, and D. I. Bush, ‘Deformation and failure modes of drystone retaining walls’, *Géotechnique*, vol. 52, no. 6, pp. 435–446, 2002.
[25] R. M. Harkness, W. Powrie, X. Zhang, K. C. Brady, and M.P. O’Reilly, ‘Numerical modelling of full-scale tests on drystone masonry retaining walls’, *Géotechnique*, vol. 50, no. 2, pp. 165–179, 2000.
[26] L. R. Alejano, M. Veiga, I. Gómez-Márquez, and J. Taboada, ‘Stability of granite drystone masonry retaining walls: II. Relevant parameters and analytical and numerical studies of real walls’, *Géotechnique*, vol. 62, no. 11, pp. 1027–1040, 2012.
[27] F. Preti, A. Errico, M. Caruso, A. Dani, and E. Guastini, ‘Dry-stone wall terrace monitoring and modelling’, *Land Degrad. Dev.*, vol. 29, no. 6, pp. 1806–1818, Jun. 2018.
[28] ENTPE, Artisans Bâtisseurs en Pierre Sèche (ABPS), Ecole des Ponts ParisTech, IFSTTAR, and Fédération Française du Bâtiment (FFB), *Technique de construction des murs en pierre sèche : Règles professionnelles*. ENTPE, Artisans Bâtisseurs en Pierre Sèche (ABPS), 2017.
[29] B. M. Das and V. K. Puri, ‘Static and dynamic active earth pressure’, *Geotech. Geol. Eng.*, vol. 14, no. 4, pp. 353–366, 1996.
[30] Y. Lin, W. Leng, G. Yang, L. Zhao, L. Li, and J. Yang, ‘Seismic active earth pressure of cohesive-frictional soil on retaining wall based on a slice analysis method’, *Soil Dyn. Earthq. Eng.*, vol. 70, pp. 133–147, 2015.

[31] M. Yazdani, A. Azad, A. hasan Farshi, and S. Talatahari, ‘Extended “Mononobe-Okabe” Method for Seismic Design of Retaining Walls’, *J. Appl. Math.*, vol. 2013, pp. 1–10, 2013.
[32] N. Mononobe and H. Matsuo, ‘On Determination of Earth Pressures during Earthquakes’, in *World Engineering Conference*, 1929, vol. 9, pp. 177–185.
[33] S. Okabe, ‘General theory on earth pressure and seismic stability of retaining wall and dam’, *Proc Civ. Engrg Soc Jpn.*, vol. 10, no. 6, pp. 1277–1323, 1924.
[34] A. Shamsabadi, S.-Y. Xu, and E. Taciroglu, ‘A generalised log-spiral-Rankine limit equilibrium model for seismic earth pressure analysis’, *Soil Dyn. Earthq. Eng.*, vol. 49, pp. 197–209, 2013.
[35] W. J. M. Rankine, ‘On the Stability of Loose Earth’, *Phil Trans R Soc Lond*, vol. 147, pp. 9–27, 1857.
[36] I. Ishibashi and Y. Fang, ‘Dynamic earth pressures with different wall movement modes’, *Soils Found.*, vol. 27, no. 4, pp. 11–22, 1987.
[37] M. Ichihara and H. Matsuzawa, ‘Earth pressure during earthquake’, *Soils Found.*, vol. 13, no. 4, pp. 75–86, 1973